Article

Not peer-reviewed version

Influence of Copigmentation on the Stability and Oxidative Stress of Anthocyanins from Purple Corn and Camu-Camu

Giulliano Najera Bless , María Victoria Muñoz Aguilar , Silvia Suarez-Cunza , Augusto Pumacahua-Ramos , Julio Cesar Santiago Contreras *

Posted Date: 30 September 2025

doi: 10.20944/preprints202509.2534.v1

Keywords: anthocyanin; copigmentation; oxidative stress; purple corn; camu-camu; resveratrol; polyaspartic acid; TBARS

 doi:10.20944/preprints202509.2534.v1

Article

Influence of Copigmentation on the Stability and Oxidative Stress of Anthocyanins from Purple Corn and Camu-Camu

Giulliano Nájera Bless [1], Victoria Muñoz Aguilar [1], Silvia Suarez-Cunza [2], Augusto Pumacahua-Ramos [3] and Julio Santiago Contreras [1,*]

[1] Departamento Académico de Química orgánica, Facultad de química e ingeniería Química, Universidad Nacional Mayor de San Marcos, Lima, Perú

[2] Departamento de Ciencias Dinámicas, Facultad de Medicina Humana, Instituto de Investigación de Bioquímica y Nutrición, Universidad Nacional Mayor de San Marcos, Lima, Perú

[3] Departamento Académico de Ingeniería de Alimentos, Universidad Nacional Intercultural de Quillabamba, Quillabamba, Perú

* Correspondence: jsantiagoc@unmsm.edu.pe

Abstract

Alzheimer's disease involves oxidative stress in brain tissue, creating a need for stable neuroprotective agents. Anthocyanins are potent antioxidants, but they are highly susceptible to degradation. This study evaluated anthocyanin from purple corn (PCA) and camu-camu (CCA) and the copigmentation effects of the phenolic acids cinnamic (C), ferulic acid (F), resveratrol (R) and polyaspartic acid (P) on the stability and neuroprotective capacity of these anthocyanins. HPLC-MS analysis identified twelve anthocyanins in PCA, including two novel compounds. Copigmentation was assessed via UV-Vis spectroscopy, FTIR, TG, and stability tests at pH 7.4. The TBARS assay evaluated protection against oxidative stress in brain tissue. Copigment R provided the strongest hyperchromic effect for PCA, while P was most effective for CCA. TG analysis showed that copigmentation with R significantly improved the thermal and pH stability of both anthocyanin sources. All single copigmented systems showed improved stability of anthocyanins in physiological conditions. Furthermore, R-copigmented anthocyanins exhibited the most potent neuroprotective effects, significantly inhibiting lipid peroxidation. Thus, copigmentation, particularly with R, is a highly effective strategy for stabilizing anthocyanins and enhancing their potential as neuroprotective agents against oxidative stress.

Keywords: anthocyanin; copigmentation; oxidative stress; purple corn; camu-camu; resveratrol; polyaspartic acid; TBARS

1. Introduction

In recent years, there has been an alarming increase in the number of people suffering from Alzheimer's disease [1]. Individuals with Alzheimer's disease experience oxidative stress in brain tissue, leading to neuronal death [2,3]. In this context, the development of novel alternatives to protect the brain from oxidative stress would be highly beneficial for treating this condition. Anthocyanins are a subclass of water-soluble flavonoids. They are characterized by the presence of a flavylium ion in their structure and exhibit colors ranging from red to blue. Purple corn (*Zea mays L.*) and camu-camu (*Myrciaria dubia*) are plant species widely cultivated in Peru. Their anthocyanin-rich extracts exhibit promising antioxidant activities [4,5]. Despite their benefits, anthocyanins are highly susceptible to degradation due to pH or temperature changes. This sensitivity limits their applications [6]. Copigmentation is a phenomenon in which a non-covalent complex forms between a pigment (anthocyanin) and a copigment (typically colorless). This process results in changes in

 doi:10.20944/preprints202509.2534.v1

optical properties (hyperchromic and/or bathochromic effects), color intensification, and enhanced anthocyanin stability [7]. Previous studies have shown that anthocyanin copigmentation can significantly improve their antioxidant activity [8–10]. The most common copigments are phenolic compounds, which facilitate π–π interactions and hydrogen bonding with anthocyanins [11]. Resveratrol (R) is a polyphenolic stilbene with strong antioxidant and neuroprotective activities. Its structure comprises two phenyl rings linked by a double bond; R exists as *trans* and *cis* isomers [12]. The planar R-*trans* isomer can interact with the flat region of the flavylium cation, favoring π-π stacking. This molecular fit can stabilize anthocyanins through face-to-face alignment, π-electron delocalization, and reduced vulnerability to water. However, R's copigmentation potential remains largely unexplored [13,14]. Additionally, anthocyanins can also form non-covalent complexes with polymers such as xanthan gum, whey protein, pectin, kappa-carrageenan, or chondroitin sulfate [12]. Polyaspartic acid (P) is a synthetic, water-soluble, non-toxic, and biodegradable polyamino acid. Structurally, P is a linear polymer composed of aspartic acid units in both L- and D-configurations, interconnected via α- and β-peptide bonds [16,17]. This unique combination of bond types and stereochemical configurations confers exceptional structural flexibility and a high density of ionizable carboxyl groups along the polymer backbone. Due to this, P acid can exhibit a high negative charge density in aqueous solution at physiological pH, which is ideal for electrostatic interactions with positively charged molecules, such as anthocyanins in their flavylium cation form. Therefore, this study aims to evaluate the copigmentation effects of anthocyanins from purple corn cob and camu-camu peel on anthocyanin stability under pH and temperature variations, as well as their protective capacity against oxidative stress in brain tissue. Known phenolic copigments—such as cinnamic acid (C), ferulic acid (F), and R—were used, along with a novel polymeric copigment, P.

2. Results and Discussion

2.1. HPLC-MS Anthocyanins Characterization

Twelve distinct anthocyanins were identified by HPLC-MS analysis in the purple corn cob extract, including two previously unreported compounds: catechin-(4,8)-peonidin-3,5-diglucoside and petunidin sophoroside. Figure 1 shows the MS spectra of these anthocyanins. The remaining ten anthocyanins matched known compounds previously documented in purple corn studies [4,18–20]. Retention times and corresponding molecular ions for all detected anthocyanins are presented in Table 1.

Table 1. Major anthocyanins identified in purple corn cob (*Zea mays L.*) extract.

Anthocyanin	Retention time (min)	Molecular ion $[M]^+$ (m/z)	MS ions (m/z)
Cyanidin-3-malonylglucoside	3.53	535	177, 287
Peonidin-3-glucoside	3.57	463	112, 286, 301, 383
Cyanidin-3-glucoside	3.64	449	167, 244, 287
Catechin-(4,8)-pelargonidin-3,5-diglucoside	3.67	883	271, 313, 407, 559, 721
Pelargonidin-3-glucoside	4.16	433	68, 130, 235, 271, 307
Catechin-(4,8)-peonidin-3,5-diglucoside	4.47	913	301, 343, 437, 589, 751
Cyanidin-3-malonylglucosyl-5-glucoside	4.52	697	177, 287, 449, 535
Pelargonidin-3-malonylglucoside	15.34	519	187, 271, 433, 475
Peonidin-3-malonylglucoside	15.76	549	185, 286, 301, 505
Pelargonidin-3-dimalonylglucoside	16.62	605	137, 177, 271, 425
Peonidin-3-dimalonylglucoside	16.81	635	137, 177, 301, 436
Petunidin sophoroside	17.57	641	145, 302, 317, 479

 doi:10.20944/preprints202509.2534.v1

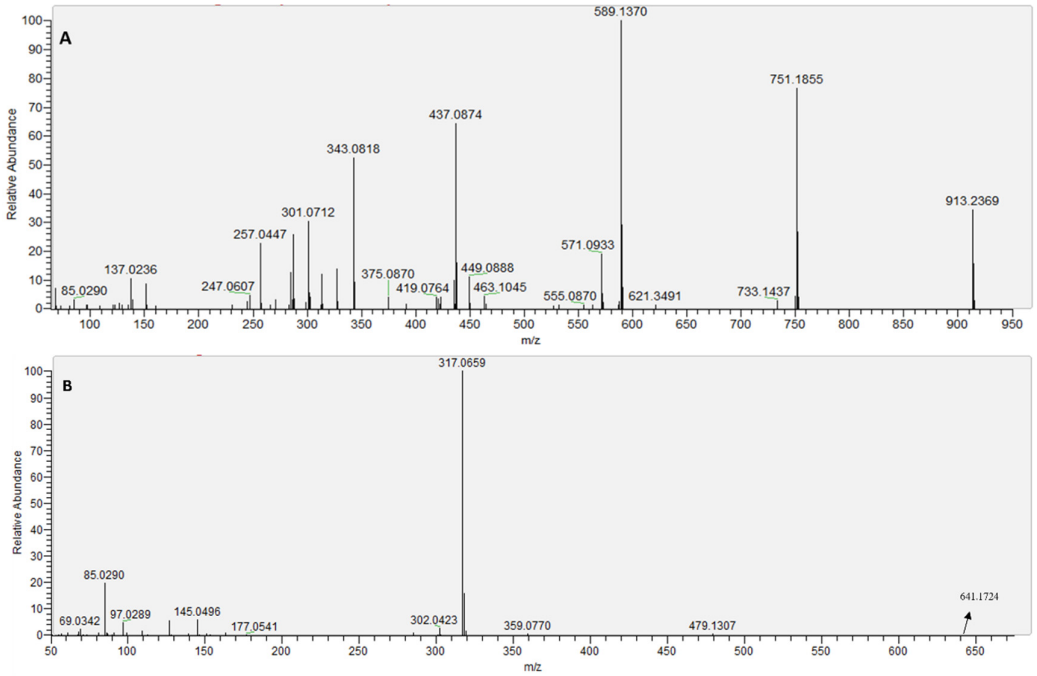

Figure 1. MS spectra of Catechin-(4,8)- peonidin 3,5-diglucoside (A) and Petunidin sophoroside (B).

The proposed structures of fragment ions of catechin-(4,8)-peonidin-3,5-diglucoside are shown in Figure 2. The initial fragmentation event involved the sequential loss of two hexose moieties (162 u each), resulting in the fragment ion at m/z 751 and the aglycone ion at m/z 589. Fragments at m/z 343, 301, and 427 are derived from the catechin moiety, as previously reported [21].

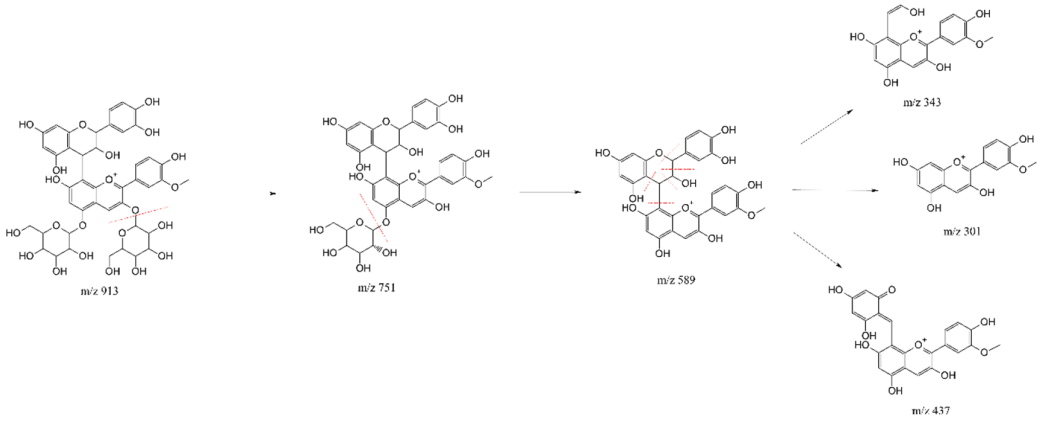

Figure 2. Proposed fragmentation pathway of catechin-(4,8)-peonidin-3,5-diglucoside.

The proposed structures of fragment ions of petunidin sophoroside are shown in Figure 3. The initial fragmentation event involved the loss of 324 u corresponding to the sophoroside moiety, generating an aglycone ion at m/z 317. A loss of 15 u was observed, corresponding to the cleavage of a $-CH_3$ group from the aglycone ion, generating the fragment ion at m/z 302. Additionally, a fragment ion at m/z 145 was observed, which is attributed to cleavages within the sophoroside moiety as reported previously [22].

 doi:10.20944/preprints202509.2534.v1

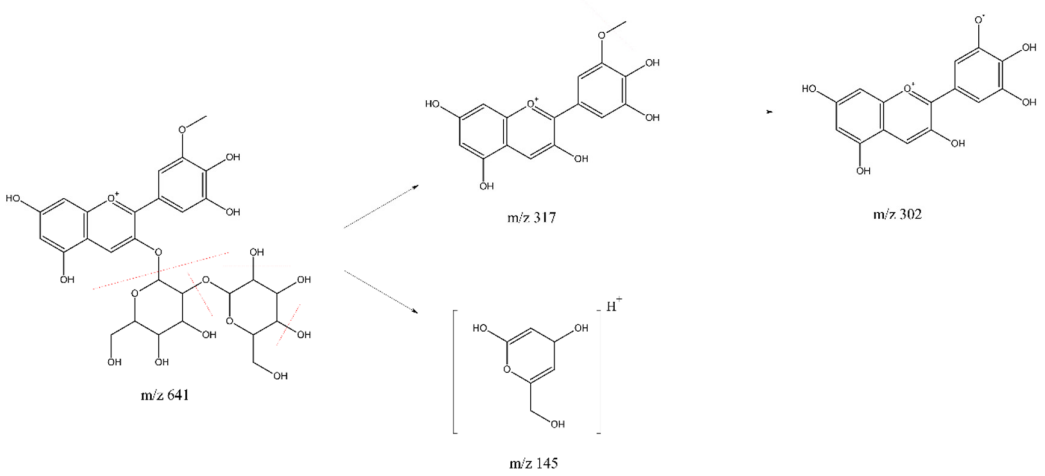

Figure 3. Proposed fragmentation pathway of petunidin sophoroside.

The HPLC-MS analysis revealed a simple anthocyanin composition in the camu-camu peel extract, identifying only two distinct anthocyanins: cyanidin 3-glucoside and delphinidin 3-glucoside. These findings are consistent with previous reports [23–25], which, to date, have not identified any additional anthocyanin structures in this botanical source. The retention times and corresponding molecular ions for both compounds are detailed in Table 2.

Table 2. Major anthocyanins identified in camu-camu peel (*Myrciaria dubia*) extract.

Anthocyanin	Retention time (min)	Molecular ion $[M]^+$ (m/z)	MS ions (m/z)
Cyanidin-3-glucoside	3.50	449	68, 153, 229, 287, 375
Delphinidin-3-glucoside	16.82	465	85, 153, 267, 303

2.2. Anthocyanins Copigmentation

2.1.1. Copigmentation with Phenolic Copigments and Polyaspartic Acid

The addition of increasing concentrations of copigments resulted in significant hyperchromic (increased absorbance) and bathochromic (red shift) effects in both purple corn cob anthocyanins (PCA) and camu-camu peel anthocyanins (CCA), demonstrating effective stabilization of the flavylium cation (Figure 4, Figures S1 and S2). For PCA copigmented samples, the maximum hyperchromic effect for each copigment was achieved at different optimal ratios (Table 4): PCA_R60 for R, PCA_F80 for F, PCA_C80 for C and PCA_P8 for P. PCA_R60 showed the most pronounced hyperchromic effect (31.37%), indicating that R acts as a superior copigment compared to F and C. However, at higher concentrations (PCA_R80), a notable decrease in maximum absorbance was observed, likely due to the destabilization of the intermolecular stacked anthocyanins [26]. The same behavior was observed in copigmentation with P: PCA_P10 with respect to PCA_P8 and CCA_P18 with respect to CCA_P16. In contrast, PCA_F80 and PCA_C80 exhibited similar hyperchromic effects (18.37% and 20.62%, respectively), suggesting comparable interaction between these phenolic acids and anthocyanins. On the other hand, PCA_C80, PCA_F80, and PCA_R60 showed identical bathochromic shifts (0.45%, 0.51%, and 0.57%, respectively). Notably, copigmentation with P produced the weakest hyperchromic effect, implying that its interactions with PCA (e.g., electrostatic or hydrogen bonding) are less effective than the π-π stacking facilitated by aromatic copigments (F, C and R). Furthermore, PCA_P8 exhibited the weakest bathochromic shift (0.16%) among all copigments.

For CCA copigmentation, the maximum hyperchromic effect for each copigment was achieved at different optimal ratios: CCA_R80 for R, CCA_F80 for F, CCA_C80 for C and CCA_P16 for P. The sample CCA_P16 exhibited the strongest hyperchromic effect (25.09%), demonstrating that P serves

 doi:10.20944/preprints202509.2534.v1

as a more effective copigment for CCA compared to R, F, and C. However, CCA_P16 showed the weakest bathochromic shift (0.19%) of all copigments. In contrast, CCA_C80, CCA_F80, and CCA_R80 (1:80 ratios for C, F, and R, respectively) showed comparable hyperchromic enhancements (9.73%, 15.70%, and 15.25%, respectively) and nearly identical bathochromic shifts (0.32%, 0.29%, and 0.32%, respectively).

Previous studies have demonstrated that aspartic acid (the monomeric unit of P) exhibits hyperchromic effects when copigmenting *Fragaria ananassa* anthocyanins [27]. Therefore, it was expected that the polymeric form (P) would similarly induce this hyperchromic effect. Furthermore, computational studies have demonstrated the feasibility of non-covalent interactions between polyaspartate and cyanidin, providing a molecular-level explanation for the observed hyperchromic shifts in copigmented systems [28]. However, minimal bathochromic shifts were observed during P copigmentation of both PCA and CCA, suggesting limited charge transfer interactions between the P polymer and the anthocyanin structures [29,30]. The copigments C and F produced similar hyperchromic and bathochromic effects for both PCA and CCA, likely due to their structural similarity as hydroxycinnamic acid derivatives. In contrast, R showed superior hyperchromic enhancement compared to C and F in PCA copigmentation, while exhibiting comparable hyperchromic and bathochromic shifts to hydroxycinnamic acid copigments in CCA stabilization. This differential behavior aligns with previous theoretical studies demonstrating R's enhanced capacity to form stable non-covalent complexes with cyanidin [13].

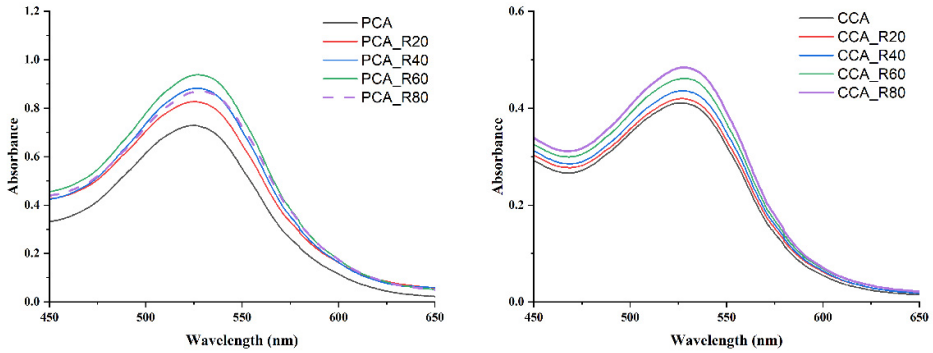

Figure 4. Visible absorption spectra of copigmented anthocyanins with resveratrol: (a) Copigmented PCA; (b) Copigmented CCA.

2.1.2. Double Copigmentation

The combination of phenolic copigments (F, C or R) with P at their optimal ratios was evaluated for dual copigmentation of anthocyanins (Table 3, Figures S1 and S2). The hyperchromic effect observed for sample PCA_RP (29.54%) was comparable to that of PCA_R60 (31.37%), indicating no synergistic enhancement when combining P with R in the PCA complex. In contrast, sample PCA_CP exhibited significantly greater hyperchromicity (49.24%) than either PCA_C80 (18.37%) or PCA_P8 (7.67%) alone. Similarly, PCA_FP showed markedly increased hyperchromic effects (51.63%) relative to its individual components (PCA_F80: 20.62%; PCA_P8: 7.67%), demonstrating that P potentiates the copigmentation efficacy of both C and F in PCA systems. While PCA_CP and PCA_FP achieved similar hyperchromic enhancements, the greater bathochromic shift in PCA_FP (0.60% vs 0.38% for PCA_CP) suggests more favorable molecular stacking of F within the ternary complex compared to C. For CCA systems, double copigmentation (CCA_CP, CCA_FP, CCA_RP) resulted in either comparable or reduced hyperchromic effects relative to single phenolic copigments. These doubly copigmented samples also displayed the smallest bathochromic shifts among all tested combinations, implying that ternary complex formation may destabilize the flavylium cation in CCA. This contrasts with previous reports of synergistic stabilization in anthocyanin-phenolic-polymer systems [31], though our findings align with documented cases where phenolic copigments compete with

 doi:10.20944/preprints202509.2534.v1

polymers for anthocyanin binding sites [32]. The differential behavior between PCA and CCA systems suggests that anthocyanin structure critically influences ternary complex formation, with P showing preferential enhancement of PCA stabilization while potentially interfering with CCA-copigment interactions.

Table 3. Hyperchromic and bathochromic effects of copigmented PCA and CCA.

PCA systems	%A	%λ	CCA systems	%A	%λ
PCA_P8	7.67 ± 0.26 ^{d}	0.16 ± 0.05 ^{d}	**CCA_P16**	25.09 ± 4.37 ^{a}	0.19 ± 0.00 ^{a}
PCA_C80	18.37 ± 1.79 ^{c}	0.45 ± 0.06 ^{bc}	**CCA_C80**	9.73 ± 0.98 ^{bcd}	0.32 ± 0.05 ^{a}
PCA_CP	49.24 ± 1.49 ^{a}	0.38 ± 0.05 ^{c}	**CCA_CP**	7.38 ± 0.51 ^{cd}	-1.08 ± 0.15 ^{c}
PCA_F80	20.62 ± 0.10 ^{c}	0.51 ± 0.00 ^{abc}	**CCA_F80**	15.70 ± 3.05 ^{b}	0.29 ± 0.00 ^{a}
PCA_FP	51.63 ± 0.64 ^{a}	0.60 ± 0.00 ^{a}	**CCA_FP**	5.43 ± 0.61 ^{d}	-0.45 ± 0.06 ^{b}
PCA_R60	31.38 ± 2.66 ^{b}	0.57 ± 0.06 ^{ab}	**CCA_R80**	15.25 ± 3.00 ^{b}	0.32 ± 0.05 ^{a}
PCA_RP	29.54 ± 1.03 ^{b}	0.57 ± 0.10 ^{ab}	**CCA_RP**	12.25 ± 0.57 ^{bc}	-0.51 ± 0.22 ^{b}

Different superscript letters in the same column indicate a significant difference at $p \leq 0.05$.

2.2. Thermogravimetric Analysis

The thermal degradation profiles of PCA and CCA revealed distinct decomposition patterns through three characteristic stages in their thermogravimetry (TG) and derivative thermogravimetry (DTG) curves (Figure 5, Tables S1 and S2). Both anthocyanin extracts showed an initial mass loss between 30-150 °C (PCA: 26.90%; CCA: 13.31%) corresponding to moisture evaporation from the sample surfaces [33]. The primary decomposition phase occurred at 150-200 °C for PCA (54.81% mass loss) and 120-220 °C for CCA (26.92% mass loss), representing thermal degradation of anthocyanin structures through deglycosylation and ring-opening reactions that yield phenolic acids and aldehydes [34]. Notably, CCA exhibited an additional decomposition stage between 300-370 °C, absent in PCA, attributed to carbonization of thermal degradation byproducts [35]. DTG analysis yielded Tmax values for the primary decomposition phase of 172.64 °C (PCA) and 184.00 °C (CCA), indicating that CCA has slightly greater inherent thermal stability. The more extensive mass loss observed for PCA during the primary decomposition indicates greater thermal lability and thus weaker thermal stability relative to CCA anthocyanins. These differential thermal behaviors suggest that structural distinctions between the two anthocyanin sources influence decomposition pathways.

Thermogravimetric analysis revealed substantial changes in the degradation patterns of anthocyanins copigmented with R, as seen in their TG and DTG curves (Figure 5, Tables S1 and S2). Both PCA_R60 and CCA_R80 showed reduced moisture loss (1.87% and 2.73%, respectively) compared to their non-copigmented counterparts, indicating enhanced surface hydrophobicity. The PCA_R60 sample exhibited glycosidic bond cleavage between 100-140 °C [35], followed by anthocyanin decomposition from 140-210 °C with 44.38% mass loss, representing a 10.43% reduction compared to native PCA. Additionally, the Tmax of PCA_R60 increased to 178.63 °C, exceeding that of non-copigmented PCA. Similarly, CCA_R80 exhibited two distinct glycosidic cleavage stages (100–130 °C and 130–155 °C) and anthocyanin decomposition occurring between 155 °C and 220 °C, with only 18.53% mass loss—significantly lower than that of native CCA. Its Tmax rose to 193.33 °C, confirming RE's stabilizing effect. The doubly copigmented systems showed slightly different behavior: PCA_RP maintained similar water loss (2.62%) and decomposition profile (41.61% mass loss at 140-210 °C) to PCA_R60, but with a marginally lower Tmax (174.14 °C). CCA_RP displayed comparable mass loss (20.67% at 130-220 °C) to CCA_R80 but with reduced Tmax (186.67 °C), suggesting that P slightly counteracts R's stabilization in ternary complexes. Notably, CCA_R80 exhibited an additional decomposition event between 220 °C and 260 °C, potentially indicating the emergence of new degradation pathways in R-CCA complexes. Residual mass analysis confirmed that R-copigmented samples consistently retained higher thermal stability compared to non-copigmented anthocyanins, with double copigmentation exhibiting similar stability to R-only

 doi:10.20944/preprints202509.2534.v1

copigmentation. Thermogravimetric analysis of PCA and CCA copigmented with P, C, and F is available in the Supplementary Materials (Figures S3–S5, Tables S1and S2).

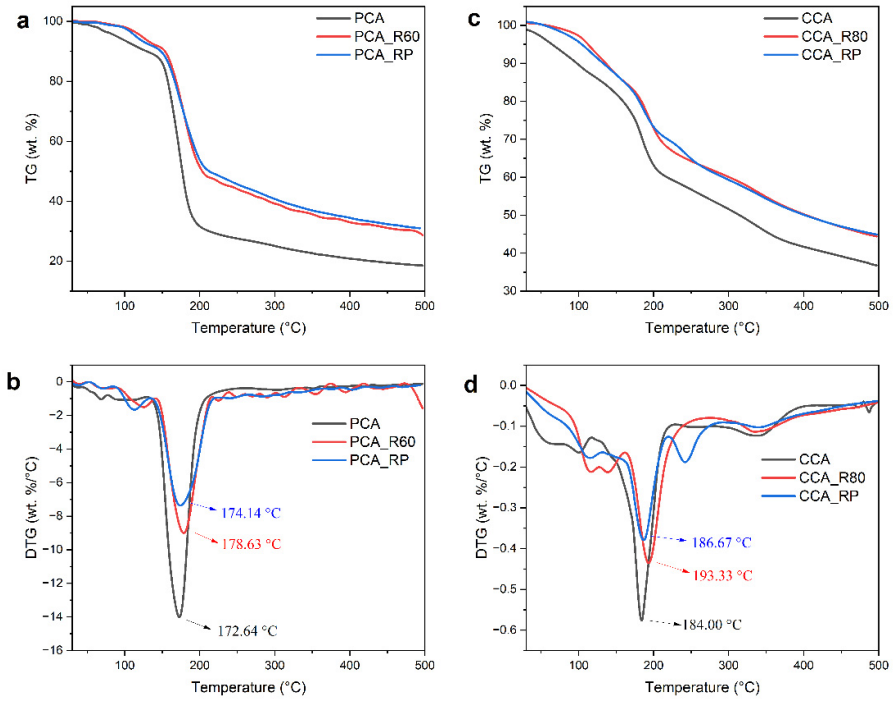

Figure 5. TG and DTG curves of copigmented anthocyanins with resveratrol: (a) TG curves of PCA, PCA_R60 and PCA_RP; (b) DTG curves of PCA, PCA_R60 and PCA_RP; (c) TG curves of CCA, CCA_R80 and CCA_RP; (d) DTG curves of CCA, CCA_R80 and CCA_RP.

As anticipated, non-copigmented PCA and CCA samples exhibited rapid thermal degradation due to destabilization of the flavylium cation. In all copigmented systems, reduced water loss was observed, suggesting the formation of hydrophobic interactions between anthocyanins and copigments that limit surface moisture adsorption. P demonstrated source-dependent stabilization: while significantly improving PCA thermal resistance, its effect on CCA was less pronounced. This is consistent with reported mechanisms whereby polymers physically encapsulate anthocyanins [32], suggesting that P may function dually as both copigment and encapsulating agent. F showed moderate stabilization of PCA but significantly enhanced CCA thermal resistance, while C paradoxically accelerated PCA degradation while protecting CCA. The observed differential effects arise because stabilization efficacy is governed by specific molecular interactions between copigment's structural characteristics and the glycosylation patterns of the anthocyanins. On the other hand, the double copigmentation demonstrated non-significant protective effects compared to single copigment formulations in all samples. Among phenolic copigments, R demonstrated superior protective effects for both PCA and CCA, attributed to its two phenolic rings connected by a styrene double bond, which closely mimics the anthocyanin backbone and provides molecular complementarity for stabilization, enabling optimal π-π stacking with the flavylium cation [36].

2.3. FTIR Analysis

The formation of hydrogen bonds and π-π interactions between anthocyanins and copigments can be identified through characteristic changes in the wavenumber and/or intensity of the functional groups involved in these non-covalent interactions (e.g., -OH, C-OH, C=O, C=C, etc.). These spectral modifications serve as evidence of non-covalent complex formation between anthocyanins and

 doi:10.20944/preprints202509.2534.v1

copigments [8,31]. The FTIR spectra of PCA and CCA revealed characteristic vibrational signatures of their molecular structures (Figure 6). The PCA spectrum exhibited key absorption bands at 3340 cm^{-1} (O-H stretching vibrations), 1723 cm^{-1} (C=O stretching indicative of the quinoidal base form), 1638 cm^{-1} (aromatic C=C stretching), 1400 cm^{-1} (C-OH bending of aromatic hydroxyl groups), and between 1228-1075 cm^{-1} (C-O-C stretching of aromatic rings) [37]. The presence of the C=O band at 1723 cm^{-1} confirms the existence of the quinoidal form in the PCA extract [38]. Similarly, the CCA spectrum showed characteristic peaks at 3419 cm^{-1} (O-H stretching), 1627 cm^{-1} (aromatic C=C stretching), 1385 cm^{-1} (aromatic C-OH bending), and in the 1146-1080 cm^{-1} range (C-O-C stretching of aromatic rings). The P spectrum (Figure 6) displayed characteristic absorption bands at 3419 cm^{-1} (O-H stretching vibrations), 1635 cm^{-1} and 1625 cm^{-1} (amide C=O stretching), 1385 cm^{-1} (O-H bending), 1147 cm^{-1} (C-O stretching), and 1119 cm^{-1} (C-N stretching) [39]. The FTIR spectrum of R (Figure 6) exhibited characteristic absorption bands at 3441 cm^{-1} (O-H stretching), 1632, 1607, 1591, 1513, and 1464 cm^{-1} (aromatic C=C stretching), 1267 cm^{-1} (C-OH bending), and 1267, 1153, 1105, and 1011 cm^{-1} (C-O stretching) [40]. Significant spectral modifications were observed in copigmented systems (Figure 6): the CCA_R80 sample showed a shifted O-H stretching band (3427 cm^{-1}) compared to pure R, while the C=O band of PCA at 1725 cm^{-1} disappeared in PCAR60, indicating preferential stabilization of the flavylium cation over the quinonoid form when complexed with R. The disappearance of R's characteristic C-O stretch at 1011 cm^{-1} and intensity reduction of the 1513 cm^{-1} C=C band in PCA_R60, along with the emergence of a new C=C band near 1400 cm^{-1} in both PCA_R60 and CCA_R80, provide evidence of hydrogen bonding and π-π interactions between anthocyanins and RE. The introduction of P in doubly copigmented systems further modified these interactions: PCA_RP showed an upshifted C=O band (1712 cm^{-1}), suggesting increased quinonoid form preference, while CCA_RP displayed an O-H band shift to 3444 cm^{-1}. Key vibrational modes underwent significant changes. The C-OH bending in PCA_RP shifted to 1266 cm^{-1}, the C-O stretch at 1107 cm^{-1} disappeared in PCA_RP, and the 1011 cm^{-1} C-O band vanished in CCA_RP. Notably, the C=C bands in PCA_RP (1630 cm^{-1}) and CCA_RP (1608 and 1592 cm^{-1}) reduced their intensity, confirming altered molecular interactions. These collective spectral changes demonstrate that P addition modifies the original hydrogen bonding and hydrophobic interactions between anthocyanins and R, likely through competitive binding and structural reorganization of the ternary complexes [32]. FTIR analysis of PCA and CCA copigmented with P, C and F can be found in Supplementary Materials (Figures S6–S8).

The comprehensive FTIR analysis of copigmented PCA and CCA systems confirms the formation of both hydrogen bonding and hydrophobic interactions involving F, C, R and P. Characteristic band shifts in the hydroxyl, carbonyl and aromatic regions provide evidence of these non-covalent interactions. The double copigmentation systems exhibited modified interaction patterns compared to single copigment complexes, particularly through changes in hydrogen bond strengths (evidenced by O-H and C=O band displacements) and π-π stacking arrangements (reflected in C=C band intensity alterations). These spectral modifications suggest that P competitively reorganizes the original interaction networks.

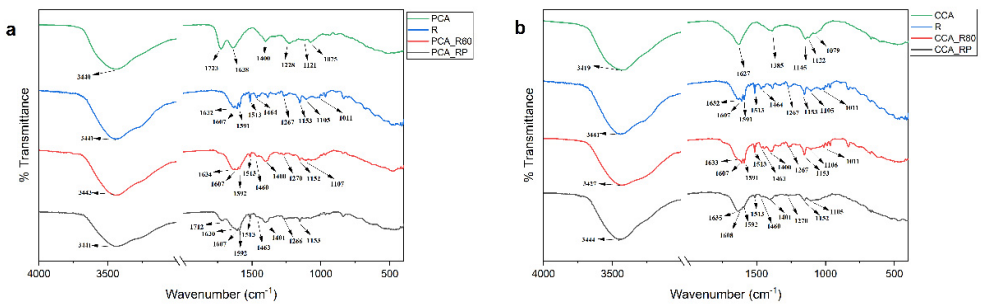

Figure 6. FTIR spectra of copigmented anthocyanins with resveratrol: (a) PCA, R, PCA_R60 and PCA_RP; (b) CCA, R, CCA_R80 and CCA_RP.

 doi:10.20944/preprints202509.2534.v1

2.4. Copigmented Anthocyanin Stability at pH 7.4

The stability of copigmented PCA and CCA under physiological conditions (pH 7.4, 37 °C) revealed significant protective effects when copigmented (Table 4). Non-copigmented controls showed the highest susceptibility to degradation, with only 24.26% (PCA) and 45.61% (CCA) of anthocyanins remaining after treatment. This aligns with established evidence that while glycosylated anthocyanins demonstrate moderate stability at physiological pH, their aglycone forms (anthocyanidins) degrade completely within 60 minutes under these conditions [41]. Phenolic copigments (F, C and R) provided substantial protection through flavylium cation stabilization via hydrophobic interactions and hydrogen bonding. The deprotonated state of F and C at physiological pH likely enhanced complex formation through electrostatic attractions [30]. At physiological pH, R remains predominantly protonated due to its relatively high pKa (>8.0) [42], distinguishing its stabilization mechanism from that of hydroxycinnamic acid copigments (F and C), which deprotonate under these conditions. This protonation state enables R to interact with anthocyanins primarily via π-π stacking and hydrogen bonding, while electrostatic interactions are not favored. These interactions are functionally comparable to those of hydroxycinnamic acids, reflected in their anthocyanin protection after treatment. On the other hand, P alone showed intermediate protection, with PCA_P8 retaining 30.17% anthocyanins (significantly better than control but inferior to phenolic copigments), while CCA_P16 performed remarkably well (51.55% retention), matching phenolic copigment efficacy. At pH 7.4, P exists in its negatively charged polyaspartate form, enabling potential electrostatic interactions with the flavylium cations of PCA and CCA anthocyanins, preventing nucleophilic water attack to the anthocyanin core [43].

Table 4. Remaining copigmented PCA and CCA after 24 h at pH 7.4 and 37 °C.

PCA systems	Remaining anthocyanins (%)	CCA systems	Remaining anthocyanins (%)
PCA	24.26 ± 1.08 ^{e}	**CCA**	45.61 ± 1.56 ^{b}
PCA_P8	30.17 ± 0.57 ^{d}	**CCA_P16**	51.55 ± 2.63 ^{a}
PCA_C80	38.82 ± 0.88 ^{bc}	**CCA_C80**	54.72 ± 1.08 ^{a}
PCA_CP	46.02 ± 0.68 ^{a}	**CCA_CP**	55.61 ± 1.49 ^{a}
PCA_F80	40.86 ± 1.39 ^{b}	**CCA_F80**	56.57 ± 2.78 ^{a}
PCA_FP	48.31 ± 1.28 ^{a}	**CCA_FP**	56.10 ± 2.19 ^{a}
PCA_R60	38.85 ± 1.49 ^{bc}	**CCA_R80**	53.92 ± 1.36 ^{a}
PCA_RP	37.16 ± 1.31 ^{c}	**CCA_RP**	55.84 ± 1.02 ^{a}

Different superscript letters in the same column indicate a significant difference at p≤0.05.

The double copigmentation demonstrated significantly enhanced protective effects compared to single copigment formulations in PCA systems. The PCA_CP system retained 46.02% of anthocyanins after degradation treatment, outperforming PCA_C80 and PCA_P8. Similarly, the PCA_FP combination showed even greater stabilization with 48.31% anthocyanin retention, surpassing all corresponding single-component systems. These results clearly demonstrate that P acts synergistically with phenolic copigments (particularly F and C) to enhance anthocyanin stability in PCA systems. The observed synergistic effect in double copigmentation systems likely arises through a sequential stabilization mechanism. Initially, the phenolic copigments (F and C) stabilize the flavylium cation through π-π stacking and hydrogen bonding interactions, as evidenced by FTIR spectral shifts. This primary stabilization maintains a higher population of positively charged flavylium cations at physiological pH than would exist in uncopigmented or P copigmented systems. The stabilized flavylium species then becomes available for enhanced electrostatic interactions with the carboxylate groups of P, creating a more stable ternary complex at physiological pH (Figure 7).

 doi:10.20944/preprints202509.2534.v1

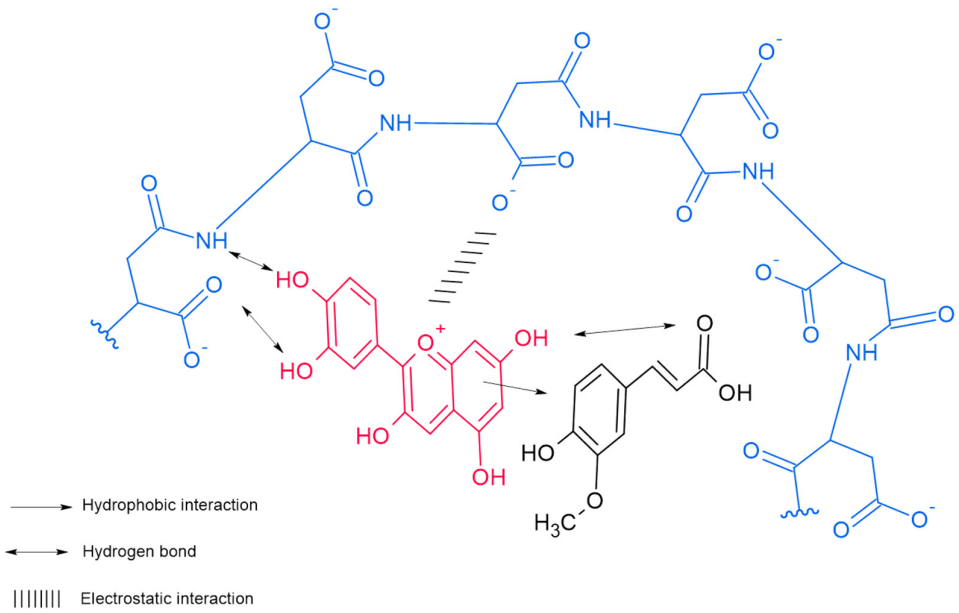

Figure 7. Ternary complex between cyanidin, ferulic acid and polyaspartate.

Consistent with prior analytical observations, no synergistic stabilization was detected in the anthocyanin retention percentages for samples PCA_RP, CCA_CP, CCA_FP and CCA_RP. While R alone showed improved protection of PCA and CCA, its combination with P failed to enhance stability beyond single-copigment performance. This suggests competitive binding between R and P for similar interaction sites on the anthocyanin structure, particularly given R's superior π-stacking capacity that may displace P's electrostatic interactions.

2.5. In Vitro Oxidative Stress Assessment by TBARS Method

The TBARS assay results demonstrated significant neuroprotective effects for both PCA and CCA against oxidative damage in brain tissue models (Table 5). All copigmented samples showed markedly reduced TBARS levels compared to the oxidative stress-induced control (SI), confirming their antioxidant capacity. The PCA extract alone exhibited substantial protection (120.56 nmol/g TBARS), while the R-copigmented sample (PCA_R60) showed exceptional performance with the lowest observed TBARS value (48.00 nmol/g). Similarly, the CCA extract demonstrated strong inherent antioxidant activity (99.50 nmol/g), with several copigmented formulations—particularly CCA_F80 (60.61 nmol/g), CCA_R80 (44.43 nmol/g), and the double copigmented combinations CCA_CP (67.82 nmol/g) and CCA_RP (40.36 nmol/g)—outperforming the control (non-stress induced). Notably, R-copigmented systems consistently showed the strongest inhibition of oxidative stress, aligning with previous reports of its neuroprotective efficacy in rat brain models [12,44].

Despite these protective effects, no synergistic interactions between anthocyanins and copigments were observed in either PCA or CCA systems. This absence of synergy may stem from the occupation of critical hydrogen bonding sites during complex formation, rendering these groups unavailable for radical scavenging activities [45]. In some cases, combinations even showed reduced efficacy—for example, CCA_P16 (97.68 nmol/g) and PCA_RP (73.28 nmol/g)—possibly due to pro-oxidant effects at high antioxidant concentrations [46]. Importantly, while copigmentation did not enhance antioxidant synergy, most copigmented samples either matched or exceeded the protection level of the non-induced stress brain control, indicating that the process successfully yields stabilized anthocyanin formulations with preserved—and in some cases enhanced—neuroprotective capacity.

 doi:10.20944/preprints202509.2534.v1

Table 5. TBARS (nmol/g) values of copigmented PCA and CCA.

Sample	TBARS (nmol/g)	Sample	TBARS (nmol/g)
Control	106.50 ± 7.70 ^{bc}	Control	106.50 ± 7.70 ^{b}
SI	172.64 ± 14.16 ^{a}	SI	172.64 ± 14.16 ^{a}
PCA systems		**CCA systems**	
P	76.12 ± 6.13 ^{d}	P	54.27 ± 11.45 ^{de}
C	83.77 ± 9.84 ^{cd}	C	98.85 ± 3.94 ^{b}
F	88.51 ± 2.91 ^{cd}	F	77.94 ± 7.76 ^{bcd}
R	51.14 ± 6.82 ^{ef}	R	44.80 ± 5.14 ^{e}
PCA	120.56 ± 7.55 ^{b}	CCA	99.50 ± 13.12 ^{b}
PCA_P8	100.90 ± 5.44 ^{bc}	CCA _P16	97.68 ± 14.14 ^{b}
PCA_C80	90.25 ± 7.28 ^{cd}	CCA _C80	77.80 ± 7.31 ^{bcd}
PCA_CP	105.48 ± 5.91 ^{bc}	CCA _CP	67.82 ± 11.24 ^{cde}
PCA_F80	115.46 ± 8.73 ^{b}	CCA _F80	60.61 ± 10.45 ^{cde}
PCA_FP	105.41 ± 9.25 ^{bc}	CCA _FP	86.47 ± 8.01 ^{bc}
PCA_R60	48.00 ± 3.72 ^{f}	CCA _R80	44.43 ± 3.03 ^{e}
PCA_RP	73.28 ± 6.78 ^{de}	CCA _RP	40.36 ± 1.46 ^{e}

Different superscript letters in the same column indicate a significant difference at $p \leq 0.05$.

3. Materials and Methods

3.1. Materials

Purple maize samples were collected in the Ayacucho region of Peru (geographical coordinates: 13°11′29.3″ S, 74°08′54.1″ W). Camu-camu fruit samples were collected in the Loreto region of Peru (geographical coordinates: 5°49′47.7″S, 76°07′10.7″W).

3.2. Extraction and Purification of Anthocyanins from Purple Corn Cob and Camu-Camu Peel

Purple corn cobs were washed and cut into approximately 5 cm × 5 cm cubes, then dried in an oven at 40 °C for 2 days until constant weight was achieved [47]. The dried purple corn cobs were ground and sieved through a N° 35 mesh. Anthocyanins were extracted using a 1:10 (w/v) ethanol/0.01% HCl solution at a 1:10 (w/v) ratio for 30 min, and then concentrated under vacuum. Ripe camu-camu fruits were washed and peeled. The peels were freeze-dried, ground, and sieved through a 35-mesh sieve [23]. Anthocyanins from camu-camu were extracted using ethanol at a 1:15 (w/v) ratio for 20 min and then concentrated under vacuum. The concentration of monomeric anthocyanins in the extracts was determined using the pH differential method [48]. The dried extracts were redissolved in distilled water (pH 2.0) and centrifuged. The supernatant was loaded onto a Lewatit S 7968 resin column to remove water-soluble impurities. Before use, the resin was pre-washed with distilled water (pH 2.0). The anthocyanin fraction was eluted with ethanol, and the solvent was removed by vacuum evaporation [49].

3.3. HPLC-MS Characterization

Three milligrams of each purified anthocyanin sample were dissolved in 3 mL of a methanolic solution (5% acetic acid) and water (5% acetic acid) in a 4:1 ratio, followed by sonication for 5 minutes. The solution was then filtered through a 0.25-µm disk filter into an HPLC vial. Chromatographic separation was performed using a Dionex Ultimate 3000 UHPLC system (Thermo Scientific) with a Luna® Omega C18 column (150 × 2.1 mm, 1.6 µm) maintained at 40 °C. The mobile phase consisted of 0.1% formic acid in water (solvent A) and 0.1% formic acid in acetonitrile (solvent B), delivered at a flow rate of 0.25 mL/min with the following gradient program: initial isocratic hold at 90% A for 1 min, linear gradient to 5% A over 22 min (1-23 min), isocratic hold at 5% A for 2 min (23-25 min), return to 90% A over 1 min (25-26 min), followed by column re-equilibration for 6 min (26-32 min). Mass spectrometric detection was performed using a Q Exactive Plus hybrid quadrupole-Orbitrap

 doi:10.20944/preprints202509.2534.v1

mass spectrometer (Thermo Scientific) operating in positive mode with a spray voltage of 2.8 kV. The ion source parameters included a capillary temperature of 280 °C, sheath gas flow rate of 40 (N_2), auxiliary gas flow rate of 10 (N_2), and heater temperature of 300 °C. Full MS scans were acquired over a mass range of 200-1500 m/z at 70,000 Resolution with an AGC target of 3×10^6 and maximum injection time of 100 ms. Data-dependent MS^2 scans were performed at 17,500 Resolution with an AGC target of 1×10^5, maximum injection time of 50 ms, and normalized collision energies of 20, 30, and 40 eV.

3.4. Anthocyanin Copigmentation

For the preparation of copigmented purple corn anthocyanins (PCA) and camu-camu anthocyanins (CCA) solutions, a previously reported methodology was followed with modifications [10]. The phenolic copigments were ferulic acid (F), cinnamic acid (C), and resveratrol (R) dissolved in ethanol, while polyaspartic acid (P) was dissolved in a pH 3.0 buffer. Equal volumes of PCA or CCA were combined with phenolic copigment solutions at different concentrations to obtain copigmented anthocyanin solutions at mass ratios of 1:20, 1:40, 1:60, and 1:80, which were then diluted with pH 3.0 buffer (e.g., PCA_F20 and CCA_F20 represent PCA-F and CCA-F at a 1:20 mass ratio, respectively). For copigmentation with P, equal volumes of PCA or CCA were mixed with P solutions at varying concentrations to achieve copigmented anthocyanin solutions at mass ratios ranging from 1:2 to 1:18, which were then diluted with ethanol (e.g., PCA_P10 and CCA_P10 represent PCA-P and CCA-P at a 1:10 mass ratio, respectively). For double copigmentation, equal volumes of PCA or CCA, phenolic copigments, and P were combined at the concentrations that yielded the highest hyperchromic and/or bathochromic effects, producing doubly copigmented anthocyanin solutions (e.g., PCA_FP and CCA_FP correspond to the optimal PCA-F-P and CCA-F-P mass ratios, respectively). All mixtures were kept in the dark at room temperature. After the copigmentation period, the solutions were analyzed by UV-Vis spectrophotometry between 450 nm and 650 nm. All samples were compared against control solutions of PCA or CCA without copigments. The effects of copigmentation were evaluated by calculating the hyperchromic and bathochromic shifts [50].

3.5. Thermogravimetric Analysis (TG) and Its Derivative (DTG)

The thermal stability of the freeze-dried samples of co-pigmented PCA and CCA was evaluated using a high-resolution thermogravimetric analyzer (TG) (TGA 5500, TA Instruments, New Castle, DE, USA) with an autosampler and equipped with a high-purity nitrogen generator (Peak Scientific Instruments Ltd., model NG3000A-220-EU). A sample of approximately 5 mg was placed in a platinum crucible and heated from 30 to 500 °C at a rate of 10 °C/min. The thermal events of the thermogravimetric curves (TG) and their derivatives (DTG) were analyzed using TRIOS™ software (version 5.4, TA Instruments) to obtain thermal parameters such as the onset temperature of decomposition, the peak degradation temperature, and the decomposed mass in each event until residue. All analyses were performed in triplicate at the Food Processing Laboratory of the National Intercultural University of Quillabamba (UNIQ), Quillabamba, Peru.

3.6. Fourier-Transform Infrared Spectroscopy (FTIR) Analysis

Freeze-dried copigmented PCA and CCA samples were homogenized with KBr and analyzed using a Nicolet iS10 FTIR spectrometer. Spectra were acquired in the range of 400 to 4000 cm^{-1} with a resolution of 4 cm^{-1}, averaging 32 scans per sample to ensure spectral clarity [10].

3.7. Copigmented Anthocyanin Stability at pH 7.4

Following the copigmentation period, the optimally copigmented PCA and CCA solutions were diluted with an equal volume of phosphate-buffered saline (PBS, pH 7.4) and adjusted as necessary to maintain consistent experimental conditions [26]. The samples were subsequently incubated in

 doi:10.20944/preprints202509.2534.v1

darkness at 37 °C under constant agitation to simulate a physiological environment. The remaining anthocyanin content was quantified at initial (0 h) and final (24 h) time points using the pH differential method.

3.8. In Vitro Oxidative Stress Assessment by TBARS Method

Chicken brains were homogenized in PBS (pH 7.4) at a 10% (w/v) concentration, followed by centrifugation (5 min, 2500 rpm, 4 °C). Oxidative stress induction was performed according to the literature protocol with modifications [51]. Briefly, 4 mM ascorbic acid (45 µL) and 2 mM $FeSO_4$ (15 µL) were mixed with 900 µL brain homogenate and 60 µL sample, followed by 30 min incubation. Subsequently, 300 µL of the reaction mixture was combined with 600 µL 10% trichloroacetic acid and heated at 100 °C for 15 min. Then, 900 µL 0.67% thiobarbituric acid was added, and the mixture was heated again at 100 °C for 30 min. After centrifugation (10 min, 7000 rpm), the absorbance of the supernatant was measured at 535 nm using UV-Vis spectrophotometry. Thiobarbituric acid reactive species (TBARS) concentration was calculated using Equation (1):

$$\frac{nmol\ TBARS}{g\ brain\ tissue} = \frac{Amp.V_t}{\varepsilon.l.V_{mp}.C_{hd}}10^9 \quad (1)$$

where A_{mp} represents the absorbance of the test sample at 535 nm, V_t is the total reaction volume (in mL), ε is the molar extinction coefficient of the malondialdehyde-thiobarbituric acid [MDA-$(TBA)_2$] complex (1.56 x10^5 $M^{-1}cm^{-1}$), l is the path length (1 cm), and C_{hd} corresponds to the brain homogenate concentration. This equation allowed for the quantification of lipid peroxidation products generated during the oxidative stress induction process.

3.9. Statistical Analysis

The results of the three independent experiments were expressed as the mean ± standard deviation. Data were analyzed by one-way ANOVA followed by Tukey's test at a 5% level of significance (p-value < 0.05).

4. Conclusions

The presence of two new anthocyanins in purple corn extracts, catechin-(4,8)-peonidin-3,5-diglucoside and petunidin sophoroside, was identified by HPLC-MS. Copigmentation with R showed greater hyperchromic effects than C and F as copigments for PCA. The polymeric copigment P demonstrated a remarkable and distinct copigmentation capacity, acting as a superior copigment for CCA and exhibiting a synergistic hyperchromic effect when combined with phenolic acids (C and F) in PCA systems. These results demonstrate that P functions as a new versatile copigment for anthocyanins. Copigmentation with R significantly improved the thermal and pH stability of both anthocyanin sources, attributed to optimal π-π stacking and hydrogen bonding with the flavylium cation, as confirmed by FTIR and TG analysis. The combination of P with phenolic copigments (C and F) further enhanced the stability of PCA at physiological pH (7.4) through the formation of a more stable ternary complex. Regarding oxidative stress, all copigmented anthocyanin formulations exhibited significant neuroprotective effects in a brain tissue model. Systems copigmented with R consistently provided the strongest protection against lipid peroxidation. The use of the copigmentation process will enable the production of more stable anthocyanin extracts with good protective activity against oxidative stress, which is expected to improve the treatment of Alzheimer's disease.

Supplementary Materials: The following supporting information can be downloaded at: Preprints.org, Figure S1: Visible absorption spectra of copigmented CCA: (a) CCA copigmented with C; (b) CCA copigmented with F; (c) CCA copigmented with P; (d) Double copigmented CCA; Figure S2: Visible absorption spectra of copigmented PCA: (a) PCA copigmented with C; (b) PCA copigmented with F; (c) PCA copigmented with P; (d) Double copigmented PCA; Figure S3: TG and DTG curves of copigmented anthocyanins with polyaspartic acid:

 doi:10.20944/preprints202509.2534.v1

(a) TG curves of PCA and PCA_P8; (b) DTG curves of PCA and PCA_P8; (c) TG curves of CCA and CCA_P16; (d) DTG curves of CCA and CCA_P16; Figure S4: TG and DTG curves of copigmented anthocyanins with cinnamic acid: (a) TG curves of PCA, PCA_C80 and PCA_CP; (b) DTG curves of PCA, PCA_C80 and PCA_CP; (c) TG curves of CCA, CCA_C80 and CCA_CP; (d) DTG curves of CCA, CCA_C80 and CCA_CP; Figure S5: TG and DTG curves of copigmented anthocyanins with ferulic acid: (a) TG curves of PCA, PCA_F80 and PCA_FP; (b) DTG curves of PCA, PCA_F80 and PCA_FP; (c) TG curves of CCA, CCA_F80 and CCA_FP; (d) DTG curves of CCA, CCA_F80 and CCA_FP; Figure S6: FTIR spectra of copigmented anthocyanins with polyaspartic acid: (a) FTIR spectra of PCA, P and PCA_P8; (b) FTIR spectra of CCA, P, CCA_P16 and CCA_P16; Figure S7: FTIR spectra of copigmented anthocyanins with cinnamic acid: (a) FTIR spectra of PCA, C, PCA_C80 and PCA_CP; (b) FTIR spectra of CCA, C, CCA_C80 and CCA_CP; Figure S8: FTIR spectra of copigmented anthocyanins with ferulic acid: (a) FTIR spectra of PCA, F, PCA_F80 and PCA_FP; (b) FTIR spectra of CCA, F, CCA_F80 and CCA_FP; Table S1: Thermal stability data of copigmented PCA; Table S2: Thermal stability data of copigmented CCA.

Author Contributions: Conceptualization, S.S.C., A.P.R. and J.S.C.; methodology, G.N.B. and V.M.A.; formal analysis, G.N.B. and V.M.A.; investigation, G.N.B. and V.M.A.; resources, S.S.C., A.P.R. and J.S.C.; writing—original draft preparation, G.N.B. and V.M.A.; writing—review and editing, S.S.C., A.P.R. and J.S.C.; visualization, G.N.B. and J.S.C.; project administration, J.S.C.; funding acquisition, J.S.C. All authors have read and agreed to the published version of the manuscript.

Funding: This research was funded by CONCYTEC/ PROCIENCIA Program, grant Contract N° PE501078236-2022-PROCIENCIA.

Data Availability Statement: Data supporting reported results can be found at https://cybertesis.unmsm.edu.pe/item/d0b7fa8a-234c-4172-a1e2-dd5fb96c4e24.

Acknowledgments: To the biologist Luis Salcedo Valdez, for his support in implementing the TBARS methodology.

Conflicts of Interest: There is no conflict of interest regarding this paper.

Abbreviations

The following abbreviations are used in this manuscript:

PCA	Purple corn cob anthocyanin
CCA	Camu-camu peel anthocyanin
C	Cinnamic acid
F	Ferulic acid
R	Resveratrol
P	Polyaspartic acid
TBARS	Thiobarbituric acid reactive species

References

1. Sara Evans-Lacko, Elisa Aguzzoli, Sanna Read, Adelina Comas-Herrera, N.F. *World Alzheimer Report 2024: Global Changes in Attitudes to Dementia*; 2024;
2. Cheignon, C.; Tomas, M.; Bonnefont-Rousselot, D.; Faller, P.; Hureau, C.; Collin, F. Oxidative Stress and the Amyloid Beta Peptide in Alzheimer's Disease. *Redox Biol.* **2018**, *14*, 450–464, doi:10.1016/j.redox.2017.10.014.
3. Persson, T.; Popescu, B.O.; Cedazo-Minguez, A. Oxidative Stress in Alzheimer's Disease: Why Did Antioxidant Therapy Fail? *Oxid. Med. Cell. Longev.* **2014**, *2014*, doi:10.1155/2014/427318.
4. Yang, Z.; Zhai, W. Identification and Antioxidant Activity of Anthocyanins Extracted from the Seed and Cob of Purple Corn (Zea Mays L.). *Innov. Food Sci. Emerg. Technol.* **2010**, *11*, 169–176, doi:10.1016/j.ifset.2009.08.012.

 doi:10.20944/preprints202509.2534.v1

5. Langley, P.C.; Pergolizzi, J. V.; Taylor, R.; Ridgway, C. Antioxidant and Associated Capacities of Camu Camu (Myrciaria Dubia): A Systematic Review. *J. Altern. Complement. Med.* **2015**, *21*, 8–14, doi:10.1089/acm.2014.0130.
6. Enaru, B.; Drețcanu, G.; Pop, T.D.; Stănilă, A.; Diaconeasa, Z. Anthocyanins: Factors Affecting Their Stability and Degradation. *Antioxidants* **2021**, *10*, doi:10.3390/antiox10121967.
7. Trouillas, P.; Sancho-García, J.C.; De Freitas, V.; Gierschner, J.; Otyepka, M.; Dangles, O. Stabilizing and Modulating Color by Copigmentation: Insights from Theory and Experiment. *Chem. Rev.* **2016**, *116*, 4937–4982, doi:10.1021/acs.chemrev.5b00507.
8. Tan, C.; Selig, M.J.; Abbaspourrad, A. Anthocyanin Stabilization by Chitosan-Chondroitin Sulfate Polyelectrolyte Complexation Integrating Catechin Co-Pigmentation. *Carbohydr. Polym.* **2018**, *181*, 124–131, doi:10.1016/j.carbpol.2017.10.034.
9. Terefe, N.S.; Netzel, G.A.; Netzel, M.E. Copigmentation with Sinapic Acid Improves the Stability of Anthocyanins in High-Pressure-Processed Strawberry Purees. *J. Chem.* **2019**, *2019*, doi:10.1155/2019/3138608.
10. He, Y.; Wen, L.; Yu, H.; Zheng, F.; Wang, Z.; Xu, X.; Zhang, H.; Cao, Y.; Wang, B.; Chu, B.; et al. Effects of High Hydrostatic Pressure-Assisted Organic Acids on the Copigmentation of Vitis Amurensis Rupr Anthocyanins. *Food Chem.* **2018**, *268*, 15–26, doi:10.1016/j.foodchem.2018.06.052.
11. Wang, J.; Zhao, Y.; Sun, B.; Yang, Y.; Wang, S.; Feng, Z.; Li, J. The Structure of Anthocyanins and the Copigmentation by Common Micromolecular Copigments: A Review. *Food Res. Int.* **2024**, *176*, doi:10.1016/j.foodres.2023.113837.
12. Constantinescu, T.; Mihis, A.G. Resveratrol as a Privileged Molecule with Antioxidant Activity. *Food Chem. Adv.* **2023**, *3*, 100539, doi:10.1016/j.focha.2023.100539.
13. Chávez, B.Y.; Paz, J.L.; Gonzalez-Paz, L.A.; Alvarado, Y.J.; Contreras, J.S.; Loroño-González, M.A. Theoretical Study of Cyanidin-Resveratrol Copigmentation by the Functional Density Theory. *Molecules* **2024**, *29*, doi:10.3390/molecules29092064.
14. Heras-Roger, J.; Alonso-Alonso, O.; Gallo-Montesdeoca, A.; Díaz-Romero, C.; Darias-Martín, J. Influence of Copigmentation and Phenolic Composition on Wine Color. *J. Food Sci. Technol.* **2016**, *53*, 2540–2547, doi:10.1007/s13197-016-2210-3.
15. Gençdağ, E.; Özdemir, E.E.; Demirci, K.; Görgüç, A.; Yılmaz, F.M. Copigmentation and Stabilization of Anthocyanins Using Organic Molecules and Encapsulation Techniques. *Curr. Plant Biol.* **2022**, *29*, doi:10.1016/j.cpb.2022.100238.
16. Sharma, S.; Dua, A.; Malik, A. Polyaspartic Acid Based Superabsorbent Polymers. *Eur. Polym. J.* **2014**, *59*, 363–376, doi:10.1016/j.eurpolymj.2014.07.043.
17. Tudorachi, N.; Chiriac, A.P. TGA/FTIR/MS Study on Thermal Decomposition of Poly(Succinimide) and Sodium Poly(Aspartate). *Polym. Test.* **2011**, *30*, 397–407, doi:10.1016/j.polymertesting.2011.02.007.
18. Yang, Z.; Zhai, W. Optimization of Microwave-Assisted Extraction of Anthocyanins from Purple Corn (Zea Mays L.) Cob and Identification with HPLC-MS. *Innov. Food Sci. Emerg. Technol.* **2010**, *11*, 470–476, doi:10.1016/j.ifset.2010.03.003.
19. Jiao, Y.; Zhang, Y.; He, Z.; Zhai, W.; Gong, H.; Yang, Z. Effect of Ferulic Acid on the Formation of Pyranoanthocyanins from Purple Corn (Zea Mays L.) Cob in a Model System and Their Effects on Color. *Int. J. Food Prop.* **2016**, *19*, 847–858, doi:10.1080/10942912.2015.1050500.
20. Paulsmeyer, M.N.; Vermillion, K.E.; Juvik, J.A. Assessing the Diversity of Anthocyanin Composition in Various Tissues of Purple Corn (Zea Mays L.). *Phytochemistry* **2022**, *201*, 113263, doi:10.1016/j.phytochem.2022.113263.
21. Berrueta, L.A.; Gallo, B.; Vicente, F. Mass Spectrometry Fragmentation Pattern of Coloured Flavanol-Anthocyanin and Anthocyanin-Flavanol Derivatives in Aged Red Wines of Rioja. **2006**, doi:10.1111/j.1755-0238.2012.00190.x.
22. Taylor, V.F.; March, R.E.; Longerich, H.P.; Stadey, C.J. A Mass Spectrometric Study of Glucose , Sucrose , and Fructose Using an Inductively Coupled Plasma and Electrospray Ionization. **2005**, *243*, 71–84, doi:10.1016/j.ijms.2005.01.001.

 doi:10.20944/preprints202509.2534.v1

23. Zanatta, C.F.; Cuevas, E.; Bobbio, F.O.; Winterhalter, P.; Mercadante, A.Z. Determination of Anthocyanins from Camu-Camu (Myrciaria Dubia) by HPLC-PDA, HPLC-MS, and NMR. *J. Agric. Food Chem.* **2005**, *53*, 9531–9535, doi:10.1021/jf051357v.
24. Fracassetti, D.; Costa, C.; Moulay, L.; Tomás-Barberán, F.A. Ellagic Acid Derivatives, Ellagitannins, Proanthocyanidins and Other Phenolics, Vitamin C and Antioxidant Capacity of Two Powder Products from Camu-Camu Fruit (Myrciaria Dubia). *Food Chem.* **2013**, *139*, 578–588, doi:10.1016/j.foodchem.2013.01.121.
25. Conceição, N.; Albuquerque, B.R.; Pereira, C.; Corr, C.G.; Lopes, C.B.; Calhelha, R.C.; Jos, M.; Barros, L.; Ferreira, I.C.F.R. By-Products of Camu-Camu [Myrciaria Dubia (Kunth) McVaugh] as Promising Sources of Bioactive High Added-Value Food Ingredients : Functionalization of Yogurts. *Molecules* **2020**, *25*, 1–17.
26. Jeong, D.; Na, K. Chondroitin Sulfate Based Nanocomplex for Enhancing the Stability and Activity of Anthocyanin. *Carbohydr. Polym.* **2012**, *90*, 507–515, doi:10.1016/j.carbpol.2012.05.072.
27. Bingöl, A.; Türkyılmaz, M.; Özkan, M. Increase in Thermal Stability of Strawberry Anthocyanins with Amino Acid Copigmentation. *Food Chem.* **2022**, *384*, doi:10.1016/j.foodchem.2022.132518.
28. Yaranga Chavez, B. Estudio DFT-TD-SCF , Docking y Dinámica Molecular Del Proceso de Copigmentación de Antocianinas , Ácidos Orgánicos y El Resveratrol . El Uso Del Poliaspartato Como Agente Encapsulante, Universidad Nacional Mayor de San Marcos, 2024.
29. Nave, F.; Brás, N.F.; Cruz, L.; Teixeira, N.; Mateus, N.; Ramos, M.J.; Di Meo, F.; Trouillas, P.; Dangles, O.; De Freitas, V. Influence of a Flavan-3-Ol Substituent on the Affinity of Anthocyanins (Pigments) toward Vinylcatechin Dimers and Proanthocyanidins (Copigments). *J. Phys. Chem. B* **2012**, *116*, 14089–14099, doi:10.1021/jp307782y.
30. Ferreira Da Silva, P.; Lima, J.C.; Freitas, A.A.; Shimizu, K.; Maçanita, A.L.; Quina, F.H. Charge-Transfer Complexation as a General Phenomenon in the Copigmentation of Anthocyanins. *J. Phys. Chem. A* **2005**, *109*, 7329–7338, doi:10.1021/jp052106s.
31. Zhao, L.; Pan, F.; Mehmood, A.; Zhang, H.; Ur Rehman, A.; Li, J.; Hao, S.; Wang, C. Improved Color Stability of Anthocyanins in the Presence of Ascorbic Acid with the Combination of Rosmarinic Acid and Xanthan Gum. *Food Chem.* **2021**, *351*, doi:10.1016/j.foodchem.2021.129317.
32. Fernandes, A.; Brás, N.F.; Oliveira, J.; Mateus, N.; De Freitas, V. Impact of a Pectic Polysaccharide on Oenin Copigmentation Mechanism. *Food Chem.* **2016**, *209*, 17–26, doi:10.1016/j.foodchem.2016.04.018.
33. Liudvinaviciute, D.; Rutkaite, R.; Bendoraitiene, J.; Klimaviciute, R.; Dagys, L. Formation and Characteristics of Alginate and Anthocyanin Complexes. *Int. J. Biol. Macromol.* **2020**, *164*, 726–734, doi:10.1016/j.ijbiomac.2020.07.157.
34. Cai, X.; Du, X.; Cui, D.; Wang, X.; Yang, Z.; Zhu, G. Improvement of Stability of Blueberry Anthocyanins by Carboxymethyl Starch/Xanthan Gum Combinations Microencapsulation. *Food Hydrocoll.* **2019**, *91*, 238–245, doi:10.1016/j.foodhyd.2019.01.034.
35. Dong, J.; Li, S.; Zhang, J.; Liu, A.; Ren, J. Thermal Degradation of Cyanidin-3-O-Glucoside: Mechanism and Toxicity of Products. *Food Chem.* **2022**, *370*, 131018, doi:10.1016/j.foodchem.2021.131018.
36. Fan, L.; Wang, Y.; Xie, P.; Zhang, L.; Li, Y.; Zhou, J. Copigmentation Effects of Phenolics on Color Enhancement and Stability of Blackberry Wine Residue Anthocyanins: Chromaticity, Kinetics and Structural Simulation. *Food Chem.* **2019**, *275*, 299–308, doi:10.1016/j.foodchem.2018.09.103.
37. Bhushan, B.; Bibwe, B.; Pal, A.; Mahawar, M.K.; Dagla, M.C.; KR, Y.; Jat, B.S.; Kumar, P.; Aggarwal, S.K.; Singh, A.; et al. FTIR Spectra, Antioxidant Capacity and Degradation Kinetics of Maize Anthocyanin Extract under Variable Process Conditions: Anthocyanin Degradation under Storage. *Appl. Food Res.* **2023**, *3*, 100282, doi:10.1016/j.afres.2023.100282.
38. Kim, H.J.; Bin, Y.T.; Karthick, S.N.; Hemalatha, K. V.; Raj, C.J.; Venkatesan, S.; Park, S.; Vijayakumar, G. Natural Dye Extracted from Rhododendron Species Flowers as a Photosensitizer in Dye Sensitized Solar Cell. *Int. J. Electrochem. Sci.* **2013**, *8*, 6734–6743, doi:10.1016/s1452-3981(23)14800-0.
39. Zegarra-Urquia, C.L.; Santiago, J.; Bumgardner, J.D.; Vega-Baudrit, J.; Hernández-Escobar, C.A.; Zaragoza-Contreras, E.A. Synthesis of Nanoparticles of the Chitosan-Poly((α,β)-DL-Aspartic Acid) Polyelectrolite Complex as Hydrophilic Drug Carrier. *Int. J. Polym. Mater. Polym. Biomater.* **2023**, *72*, 497–506, doi:10.1080/00914037.2022.2029440.

 doi:10.20944/preprints202509.2534.v1

40. Güder, A.; Korkmaz, H.; Gökce, H.; Alpaslan, Y.B.; Alpaslan, G. Isolation, Characterization, Spectroscopic Properties and Quantum Chemical Computations of an Important Phytoalexin Resveratrol as Antioxidant Component from Vitis Labrusca L. and Their Chemical Compositions. *Spectrochim. Acta - Part A Mol. Biomol. Spectrosc.* **2014**, *133*, 378–395, doi:10.1016/j.saa.2014.05.056.
41. Fleschhut, J.; Kratzer, F.; Rechkemmer, G.; Kulling, S.E. Stability and Biotransformation of Various Dietary Anthocyanins in Vitro. *Eur. J. Nutr.* **2006**, *45*, 7–18, doi:10.1007/s00394-005-0557-8.
42. López-Nicolás, J.M.; García-Carmona, F. Aggregation State and PKa Values of (E)-Resveratrol as Determined by Fluorescence Spectroscopy and UV-Visible Absorption. *J. Agric. Food Chem.* **2008**, *56*, 7600–7605, doi:10.1021/jf800843e.
43. Cahyana, Y.; Gordon, M.H. Interaction of Anthocyanins with Human Serum Albumin: Influence of PH and Chemical Structure on Binding. *Food Chem.* **2013**, *141*, 2278–2285, doi:10.1016/j.foodchem.2013.05.026.
44. Menegas, S.; Ferreira, C.L.; Cararo, J.H.; Gava, F.F.; Dal-Pont, G.C.; Gomes, M.L.; Agostini, J.F.; Schuck, P.F.; Scaini, G.; Andersen, M.L.; et al. Resveratrol Protects the Brain against Oxidative Damage in a Dopaminergic Animal Model of Mania. *Metab. Brain Dis.* **2019**, *34*, 941–950, doi:10.1007/s11011-019-00408-1.
45. Bayram, I.; Decker, E.A. Underlying Mechanisms of Synergistic Antioxidant Interactions during Lipid Oxidation. *Trends Food Sci. Technol.* **2023**, *133*, 219–230, doi:10.1016/j.tifs.2023.02.003.
46. Rajashekar, C.B. Dual Role of Plant Phenolic Compounds as Antioxidants and Prooxidants. *Am. J. Plant Sci.* **2023**, *14*, 15–28, doi:10.4236/ajps.2023.141002.
47. Jing, P.; Giusti, M.M. Effects of Extraction Conditions on Improving the Yield and Quality of an Anthocyanin-Rich Purple Corn (Zea Mays L.) Color Extract. *J. Food Sci.* **2007**, *72*, 363–368, doi:10.1111/j.1750-3841.2007.00441.x.
48. Lee, J.; Durst, R.W.; Wrolstad, R.E. Determination of Total Monomeric Anthocyanin Pigment Content of Fruit Juices, Beverages, Natural Colorants, and Wines by the PH Differential Method: Collaborative Study. *J. AOAC Int.* **2005**, *88*, 1269–1278, doi:10.1093/jaoac/88.5.1269.
49. Rodriguez-Lopez, A.D.; Reig, M.; Mayor, L.; Ortiz-Climent, M.; Garcia-Castello, E.M. Characterization of Ionic Exchange and Macroporous Resins for Their Application on the Separation and Recovery of Chlorogenic Acid from the Wastewater of Artichoke Blanching. *Sustain.* **2021**, *13*, doi:10.3390/su13168928.
50. Kanha, N.; Surawang, S.; Pitchakarn, P.; Regenstein, J.M.; Laokuldilok, T. Copigmentation of Cyanidin 3-O-Glucoside with Phenolics: Thermodynamic Data and Thermal Stability. *Food Biosci.* **2019**, *30*, 100419, doi:10.1016/j.fbio.2019.100419.
51. Buege, J.A.; Aust, S.D. Microsomal Lipid Peroxidation. *Methods Enzymol.* **1978**, *52*, 302–310.
52. Kalinowska, M.; Świsłocka, R.; Lewandowski, W. The Spectroscopic (FT-IR, FT-Raman and 1H, 13C NMR) and Theoretical Studies of Cinnamic Acid and Alkali Metal Cinnamates. *J. Mol. Struct.* **2007**, *834–836*, 572–580, doi:10.1016/j.molstruc.2006.11.043.
53. Hanai, K.; Kuwae, A.; Takai, T.; Senda, H.; Kunimoto, K.K. Comparative Vibrational and NMR Study of Cis-Cinnamic Acid Polymorphs and Trans-Cinnamic Acid. *Spectrochim. Acta - Part A Mol. Biomol. Spectrosc.* **2001**, *57*, 513–519, doi:10.1016/S1386-1425(00)00401-7.
54. Sebastian, S.; Sundaraganesan, N.; Manoharan, S. Molecular Structure, Spectroscopic Studies and First-Order Molecular Hyperpolarizabilities of Ferulic Acid by Density Functional Study. *Spectrochim. Acta - Part A Mol. Biomol. Spectrosc.* **2009**, *74*, 312–323, doi:10.1016/j.saa.2009.06.011.